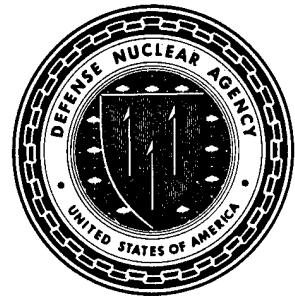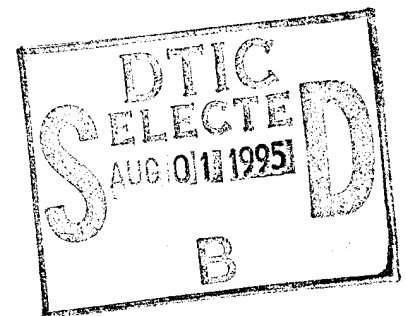Defense Nuclear Agency
Alexandria, VA 22310-3398

Simulation Study of Shocked Particle Velocity Distributions in a HANE Disturbed Plasma

Nevel T. Gladd
Stephen H. Brecht
Berkeley Rsch Associates, Inc.
P.O. Box 241
Berkeley, CA 94701-0241

DTIC
SELECTED
AUG 01 1995
B

August 1995

Technical Report

19950731 140

DTIC QUALITY INSPECTED 5

DISTRIBUTION LIST UPDATE

This mailer is provided to enable DNA to maintain current distribution lists for reports. (We would appreciate your providing the requested information.)

☐ Add the individual listed to your distribution list.

☐ Delete the cited organization/individual.

☐ Change of address.

> **NOTE:**
> Please return the mailing label from the document so that any additions, changes, corrections or deletions can be made easily. For distribution cancellation or more information call DNA/IMAS (703) 325-1036.

NAME: _____

ORGANIZATION: _____

OLD ADDRESS	**CURRENT ADDRESS**
_____	_____
_____	_____
_____	_____

TELEPHONE NUMBER: ( ) _____

DNA PUBLICATION NUMBER/TITLE	**CHANGES/DELETIONS/ADDITIONS, etc.)** *(Attach Sheet if more Space is Required)*
_____	_____
_____	_____
_____	_____

DNA OR OTHER GOVERNMENT CONTRACT NUMBER: _____

CERTIFICATION OF NEED-TO-KNOW BY GOVERNMENT SPONSOR (if other than DNA):

SPONSORING ORGANIZATION: _____

CONTRACTING OFFICER OR REPRESENTATIVE: _____

SIGNATURE: _____

CUT HERE AND RETURN

DEFENSE NUCLEAR AGENCY
ATTN: IMAS
6801 TELEGRAPH ROAD
ALEXANDRIA, VA   22310-3398

REPORT DOCUMENTATION PAGE

1. AGENCY USE ONLY (Leave blank)	2. REPORT DATE 950801	3. REPORT TYPE AND DATES COVERED Technical 931001 – 941001

4. TITLE AND SUBTITLE

Simulation Study of Shocked Particle Velocity Distributions in a HANE Disturbed Plasma

5. FUNDING NUMBERS

C - DNA 001-92-C-0116
PE - 62715H
PR - AF
TA - AN
WU- DH321420

6. AUTHOR(S)

Nevel T. Gladd and Stephen H. Brecht

7. PERFORMING ORGANIZATION NAME(S) AND ADDRESS(ES)
Berkeley Rsch Associates, Inc.
P.O. Box 241
Berkeley, CA 94701-0241

8. PERFORMING ORGANIZATION REPORT NUMBER

BRA-94-369R

9. SPONSORING/MONITORING AGENCY NAME(S) AND ADDRESS(ES)
Defense Nuclear Agency
6801 Telegraph Road
Alexandria, VA 22310-3398
RAEM/Prasad

10. SPONSORING/MONITORING AGENCY REPORT NUMBER

DNA-TR-94-161

13. ABSTRACT *(Maximum 200 words)*

A two dimensional, hybrid particle-in-cell simulation code is used to study the velocity distributions of a plasma disturbed by a collisionless shock wave generated by a high altitude nuclear explosion. Knowledge of the velocity distributions is crucial in understanding plasma instabilities that thermalize the disturbed plasma and produce the ion deposition spectrum. Variation in the deposition spectrum can cause orders of magnitude differences in IR radiation and ionization and strongly affect systems. The simulations indicate that the relevant anisotropic velocity distributions are shell-like rather than bimax wellian. Since almost all theoretical analysis of thermalizing plasma instabilities have been based on bimaxwellian distributions, this research motivates a reexamination of thermalizing instabilities using velocity distributions that are more physically realistic.

14. SUBJECT TERMS

HANE	Plasma
Simulation	Velocity Distribution

15. NUMBER OF PAGES
30

16. PRICE CODE

17. SECURITY CLASSIFICATION OF REPORT UNCLASSIFIED	18. SECURITY CLASSIFICATION OF THIS PAGE UNCLASSIFIED	19. SECURITY CLASSIFICATION OF ABSTRACT UNCLASSIFIED	20. LIMITATION OF ABSTRACT SAR

CLASSIFIED BY:

N/A since Unclassified.

DECLASSIFY ON:

N/A since Unclassified.

CONVERSION TABLE

Conversion factors for U.S. customary to metric (SI) units of measurement.

To convert from	to	Multiply by
angstrom	meters (m)	$1.000\ 000 \times 10^{-10}$
atmosphere (normal)	kilo pascal (kPa)	$1.013\ 25 \times 10^{+2}$
bar	kilo pascal (kPa)	$1.000\ 000 \times 10^{+2}$
barn	meter^2 (m^2)	$1.000\ 000 \times 10^{-28}$
British thermal unit (thermochemical)	joule (J)	$1.054\ 350 \times 10^{+3}$
cal (thermochemical)/ cm^2	mega joule/m^2 (MJ/m^2)	$4.184\ 000 \times 10^{-2}$
calorie (thermochemical)	joule (J)	$4.184\ 000 \times 10^{+3}$
curie	giga becquerel (GBq)	$3.700\ 000 \times 10^{+1}$
degree Celsius	degree kelvin (K)	$t_K = t^\circ{}_C + 273.15$
degree (angle)	radian (rad)	$1.745\ 329 \times 10^{-2}$
degree Fahrenheit	degree kelvin (K)	$t_K = (t^\circ{}_F + 459.67)/1.8$
electron volt	joule (J)	$1.602\ 19 \times 10^{-19}$
erg	joule (J)	$1.000\ 000 \times 10^{-7}$
erg/second	watt(W)	$1.000\ 000 \times 10^{-7}$
foot	meter (m)	$3.048\ 000 \times 10^{-1}$
foot-pound-force	joule (J)	$1.355\ 818$
gallon (U.S.liquid)	meter^3 (m^3)	$3.785\ 412 \times 10^{-3}$
Gauss	Tesla	$1.000\ 000 \times 10^{-4}$
inch	meter (m)	$2.540\ 000 \times 10^{-2}$
joule/kilogram (J/kg) (radiation dose absorbed)	gray (Gy)	$1.000\ 000$
kilotons	terajoules	4.183
kip (1000 1 bf)	newton (N)	$4.448\ 222 \times 10^{+3}$
kip/inch^2 (ksi)	kilo pascal (kPa)	$6.894\ 757 \times 10^{+3}$
ktap	newton-second/m^2 (N-s/m^2)	$1.000\ 000 \times 10^{+2}$
micron	meter (m)	$1.000\ 000 \times 10^{-6}$
mil	meter (m)	$2.540\ 000 \times 10^{-5}$
mile (international)	meter (m)	$1.609\ 344 \times 10^{+3}$
ounce	kilogram (kg)	$2.834\ 952 \times 10^{-2}$
pound-force (1bf avoirdupois)	newton (N)	$4.448\ 222$
pound-force inch	newton-meter (N-m)	$1.129\ 848 \times 10^{-1}$
pound-force/inch	newton/meter (N/m)	$1.751\ 268 \times 10^{+2}$
pound-force/foot^2	kilo pascal (kPa)	$4.788\ 026 \times 10^{-2}$
pound-force/inch^2 (psi)	kilo pascal (kPa)	$6.894\ 757$
pound-mass (1bm avoirdupois)	kilogram (kg)	$4.535\ 924 \times 10^{-1}$
pound-mass-foot^2 (moment of inertia)	kilogram-meter^2(kg·m^2)	$4.214\ 011 \times 10^{-2}$
rad (radiation dose absorbed)	gray (Gy)	$1.000\ 000 \times 10^{-2}$
roentgen	coulomb/kilogram (C/kg)	$2.579\ 760 \times 10^{-4}$
shake	second (s)	1.000×10^{-8}
slug	kilogram (kg)	$1,459\ 390 \times 10^{+1}$
torr (mm Hg, O$^\circ$ C)	kilo pascal (kPa)	$1.333\ 22 \times 10^{-1}$

TABLE OF CONTENTS

FIGURES

SECTION 1
INTRODUCTION

The deposition of energetic air and debris ions in the altitude range of 100-150 km is a major cause of IR, C^3, and radar system degradation. Variations in the energy spectrum of the deposited particles can cause orders of magnitude differences in IR radiation and ionization. If the spectrum is "soft", ions are deposited at high altitude and produce long lived ionization because of the low recombination rate. However, the IR radiation will be lower because there are fewer molecules. If the spectrum is "hard", deposition will occur at lower altitudes (105-120 km). The ionization will be short lived but the IR radiation will be more intense because there are more excited molecules.

Current systems codes predictions depend upon realistic and reliable predictions of deposition spectra. The research under this contract is focused on providing the first principles calculations necessary to provide a better understanding of the acceleration and interaction processes between the expanding debris and the ionosphere of the earth. This report describes evolutionary steps toward an improved ion deposition model for DNA's system codes.

A two dimensional, hybrid particle-in-cell simulation code is used to study the velocity distributions of a plasma disturbed by a collisionless shock wave generated by a high altitude nuclear explosion. Knowledge of the velocity distributions is crucial in understanding plasma instabilities that thermalize the disturbed plasma and produce the ion deposition spectrum that causes strong system effects. It is found that plasma particles are strongly accelerated when first encountering the shock wave. Rather than being specularly reflected, particles are scattered in various directions with respect to the shock because of irregularities in the shock front. On the basis of studies of velocity distributions at points successively deeper into the shock, it is found that the beam-like velocity distribution of particles in front of the shock is changed, over a relatively short distance, into a form gyrotropic with respect to the magnetic field. Over a longer distance scale the velocity distribution is partially isotropized, developing a Maxwellian shape in the component parallel to the magnetic field. In contrast, the perpendicular component maintains a shell-like rather than Maxwellian shape. This observed velocity distribution differs substantially from the bimaxwellian form typically used in analyses of plasmas disturbed by a collisionless shock. For example, bimaxwellian velocity distributions are assumed in the models used by codes such as CMHD.

The initial flow of kinetic energy is radial as debris expands away from the detonation point. The debris material expands faster than the local Alfven velocity, $V_A = B/(4\pi \eta m_i)^{1/2}$ and generates a collisionless shock wave which energizes the background ionospheric plasma. Since the expanding shock wave pushes the Earth's magnetic field in front of it, much initial energization of the ionospheric plasma is perpendicular to the local magnetic field. It is the process by which energy is isotropized with respect to the magnetic field that especially interests us since the parallel energy can readily flow down along field lines and be deposited in the atmosphere. Ultimately, we seek a "turning model" -- a parameterized model of how energy that is initially predominantly perpendicular

to field lines is "turned" into parallel energy.

It is well known from kinetic theory that plasmas with free energy will develop unstable motions and relax to a lower energy state. A classic example is a plasma with more kinetic energy perpendicular to the magnetic field than kinetic energy parallel to the field. Such a plasma is said to be anisotropic, with $T_\perp > T_\parallel$, and is subject to instabilities such as the mirror mode [Chandrasekhar, 1958; Barnes, 1966; Hasegawa, 1975] or the Alfven ion cyclotron [Kennel and Petschek, 1966; Davidson and Ogden, 1975]. These instabilities develop nonlinearly so as to reduce the temperature anisotropy of the plasma. The mirror mode and Alfven ion cyclotron are both observed in magnetosheath [Tsurutani et al., 1982; Moustaizis et al., 1986; Hubert et al., 1989; Sckopke et al., 1990, Brinca et al., 1990; Anderson and Fuselier, 1992], behind the collisionless bow shock that develops when the super-Alfvenic solar wind flow encounters the earth. They have been widely studied, with both theory and simulation, as probable mechanisms for thermalizing ion distributions in the magnetosheath [Gary et al., 1976, 1992; Tajima et al., 1977; Ambrosiano and Brecht, 1987; Winske and Quest, 1988; Brinca et al., 1990; Yoon, 1992; McKean et al., 1992]

The collisionless shock associated with a HANE is a dynamic event and differs from the quasi-stationary bow shock. A HANE produced shock is initially driven quite strongly but the impetus diminishes as the expanding debris material gives up its energy to the background. The bow shock is continuously driven by the solar wind. This difference has consequences for the development of plasma instabilities that isotropize the shock disturbed plasma. In the case of the bow shock, it is adequate to model the shocked plasma with a bimaxwellian velocity distribution function for which $T_\perp > T_\parallel$. In contrast, the dynamical, HANE induced, collisionless shock may have velocity space distortions of the distribution function in addition to the temperature anisotropy.

In this report we describe the use of a two-dimensional hybrid particle-in-cell simulation to ascertain the characteristic shape of the shocked plasma velocity distribution functions. It is found that plasma particles are strongly accelerated when first encountering the shock wave. Rather than being specularly reflected, particles are scattered in various directions with respect to the shock because of irregularities in the shock front. On the basis of studies of velocity distributions at points successively deeper into the shock, it is found that the beam-like velocity distribution of particles in front of the shock is changed, over a relatively short distance, into a form gyrotropic with respect to the magnetic field. Over a longer distance scale the velocity distribution is partially isotropized, developing a Maxwellian shape in the component parallel to the magnetic field. In contrast, the perpendicular component maintains a shell-like rather than Maxwellian shape. This observed velocity distribution differs substantially from the bimaxwellian form typically used in analyses of plasmas disturbed by a collisionless shock.

In Section II we describe the 2-D hybrid PIC code and demonstrate how it is used to generate a collisionless shock typical of that produced by a HANE. The description of the macroscopic features of the shock, the nature of particle orbits in the presence of the shock, and the spatial evolution of the velocity distribution function within the shocked plasma are described in Section III. The observed velocity distribution function is characterized by an analytical distribution in Section IV and

the method by which the analytical distribution is fitted to observations is described. Some properties of the fitting analytical distribution are also presented. Conclusions are drawn in Section V.

The implications of the observed velocity distribution functions for the mirror mode and Alfven ion cyclotron instabilities in a HANE disturbed plasma are examined in a separate report [Gladd and Brecht, 1994].

SECTION 2
DESCRIPTION OF SIMULATION

We are interested in the shape of the velocity distribution functions of ions energized by the passage of a typical, HANE induced, collisionless shock wave. To model such a shocked plasma we use a two-dimensional, hybrid particle-in-cell simulation code that treats plasma ions kinetically while treating electrons as a fluid. The details of the code are described in [Thomas and Brecht, 1986; Brecht and Thomas, 1988].

The collisionless shock is created in the simulation by streaming a light mass plasma onto a much heavier obstacle plasma. A shock wave is generated at the obstacle and flows back upstream into the light plasma. The shock formation process is dynamic and the simulation terminates when the shock wave has propagated across the computational grid. This situation is illustrated in Figure 2-1a. This method has some advantages over propagating the light plasma into a back wall [Winske and Quest, 1988] since the boundary conditions at the back wall are not involved. The simulation geometry is shown in Figure 2-1b. The simulation plane is the two-dimensional (x-z) plane. The ambient magnetic field is in the +x-direction, and perpendicular to the ambient flow (+z- direction) and the direction of propagation of the shock wave (-z-direction).

The particular simulation we discuss in this report is designed to produce a collisionless shock representative of a HANE. In Figure 2-2 we show representative profiles of the simulated collisionless shock at four different times (0, 500, 1000, 2000 Δt) during the simulation. The thick solid line represents the background material (n_b, A = 54, Fe^+). The dashed line represents the lighter material that is flowing to the right (n_l, A = 16, O^+). The thin solid line represents the magnetic field. Here, B_x and n_i have been averaged in the x direction and plotted as a function of z. These quantities have also been normalized to their values upstream of the shock. In this figure, the light material flows to the right and a shock develops when it encounters the stationary heavy material. This shock then propagates to left. After some transient development time, the characteristic overshoots of density and magnetic field develop, as does a small foot region on the density that corresponds to ions being reflected from the shock.

4
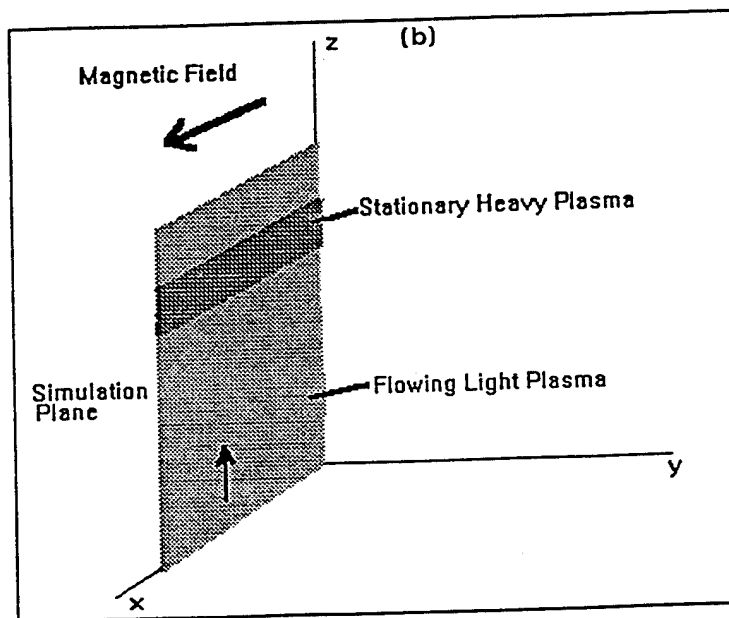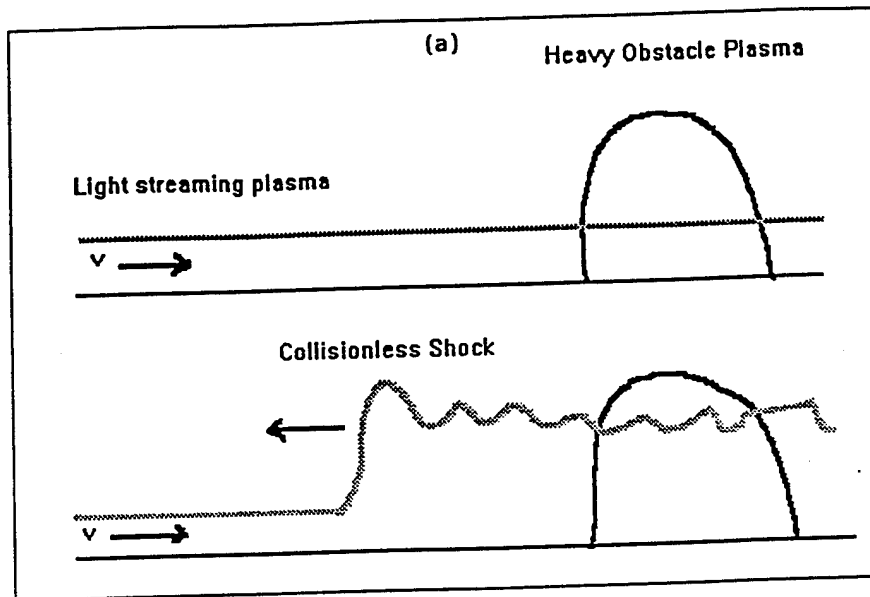
Figure 2-1. a) Method for generating collisionless shock with simulation. A light specie is flowed onto a heavy specie, the shock develops and propagates upstream.
b) Geometry of the simulation. Simulation plane is x-z, magnetic field in x direction, and initial flow is in the -z direction.

Figure 2-2.   a) Profiles of main magnetic field component, B_x, light plasma density, n_i, and heavy plasma density, n_h, as a function of z. Profiled quantities are averaged in the x-direction. Snapshots taken after 0, 500, 1000 and 2000 time steps.

6

The parameters characterizing this simulation are

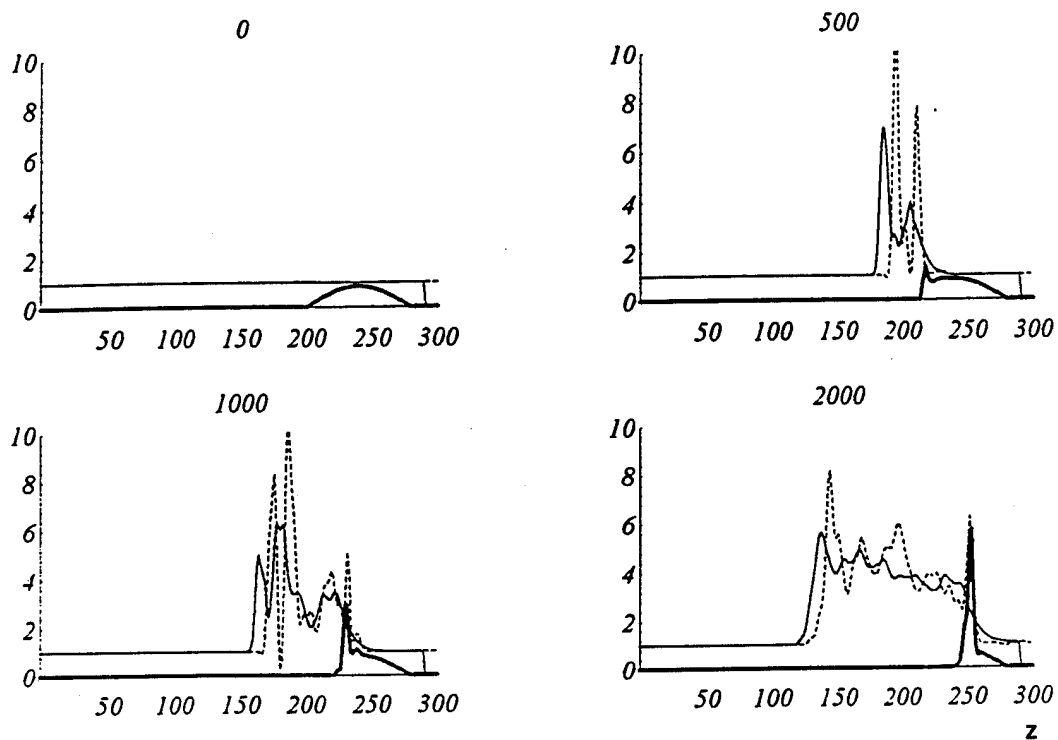|	
N_x (cells in x-direction)	32
N_z (cells in z-direction)	200
dx (cell size in x-direction)	1.5 km
dz (cell size in z-direction)	1.5 km
B_{x0} (ambient B field)	0.1 Gauss
n_{H0} (density of heavy specie A = 54, Fe^+)	$2.14\ 10^6$ cm^{-3} (16384)
n_{L0} (density of light specie A = 16, O^+)	$6.00\ 10^4$ cm^{-3} (51200)
v_{zL0} (drift speed of light specie)	2000 km/sec
Z_H	1
Z_L	1
Δt	$1.0\ 10^{-4}$ sec
ω_{ci}	60 sec^{-1}
ρ_i	33 km
c/ω_{pi}	3.7 km

For these parameters the collisionless shock has Mach number 9.0, calculated as the ratio of v_{zL0}/v_{AL0} with v_{AL0} the Alfven speed in the light specie.

SECTION 3
ANALYSIS OF SIMULATION

Individual particle behavior: We first consider the behavior of simulation particles as they encounter the shock wave (see Figure 3-1). Here we show the positions of individual particles in a 4 cell × 20 cell region of the simulation. The simulation time is 2000 time steps and the z-strip shown starts with cell z = 84 (the front of the shock) and runs through cell z = 124 (well into the shock). The x-strip contains the central cells 15, 16, 17, 18 and are taken to be representative of the 32 simulation cells transverse to the direction of shock propagation. The regular spacing of particles at the bottom of Figure 3-1 corresponds to the uniform light particles (O^+) propagating upward at a velocity of 2000 km/sec. The top of the Figure is well into the shocked region and the particles have been scattered by the turbulent electric and magnetic fields. The temporal and spatial variation of these turbulent fields is slow with respect to the velocity of the incoming particles so the sequence in space of incoming particles appears like a tracer in time of an individual particle. In this respect, we see that some of the incoming particles are strongly reflected back in the direction from which they came. Such reflection is expected for a high Mach number collisionless shock wave. This method of viewing particles is of limited utility in determining the overall effects of the shock on the plasma. It is more instructive to consider the shape of the velocity distribution function of the particles.

Evolution of velocity distribution functions: We are particularly interested in the change of the particle distribution function at successively greater penetration distances into to the shock. It is instructive to consider the distribution function with both spherical and cylindrical representations.

Some observed spherical velocity distribution functions are illustrated in Figure 3-2. The velocity of an individual particle is characterized by the magnitude of the velocity $|v|$ and the spherical angles θ (the polar angle) and ϕ (the azimuthal angle). The orientation of the coordinate system is such that $\theta = 0$ points in the +x direction (the direction of the ambient magnetic field) and $\phi = 0$ points in the +z direction (the direction of ambient particle inflow). We have chosen to display the angular distribution in a planar form by unwrapping θ and ϕ from a sphere. Thus θ has the extent ($0 < \theta < \pi$) and ϕ has the extent ($0 < \phi < 2\pi$). To clarify what we have done, the actual spherical representation is shown in Figure 3-3 where $f(|v|, \theta, \phi)$. Figure 3-3a) illustrates what a beam distribution would look like in a spherical representation; figure 3-3b) illustrates what a gyrotropic distribution would look like. Gyrotropic means that the distribution does not depend on the azimuthal angle ϕ. In constructing the distribution function for a given value of z we include all particles in 2 cell spatial z region starting with that value of z and the full 32 cell x region. Thus a given distribution is calculated with all of the particle in 2 × 32 cell region. Figure 3-2a corresponds to a position z = cell 84 near the shock front and 614 particles are used to construct the distribution functions. In this front region most particles have not yet been disturbed by the shock and have a velocity of 2000 km/sec. In the corresponding plot of the angular distribution, these largely undisturbed particles show up as a spike at $\phi = 0$. The periodic symmetry of the planar display $\phi = 0 = 2\pi$ makes it appear as if there were two spikes. The situation actually corresponds to that shown in Figure 3-3a). Also in Figure 3-2a) we see that a small number of particles have been accelerated to velocities of order 3000

8

km/sec. Inspection of the angular distribution shows that these particles are grouped near $\phi = \pi$, $\theta = \pi/2$ and thus correspond to reflected particles. Figure 3-2b) corresponds to a z value two cells deeper into the shock region where 935 particles are contributing to the illustrated distribution. Since we are only interested in the change of the shape of the distribution functions, all of them have been normalized to the same ordinate value. At z = cell 88 we see that the distributions of velocity magnitudes have been further scattered with a net slowing below the initial velocity of 2000 km/sec. In Figure 3-2c), at cell z = 92 where 1897 particles are included, this slowing and scattering of the distribution of velocity magnitudes is even more prominent. In addition, we see that a strong angular scattering in ϕ has occurred. The shock turbulence is driving the angular distribution of the particles toward gyrotropy with respect to the direction of the magnetic field.

The spherical representation of the particle distribution function is not convenient for stability analyses involving an ambient magnetic field. We need to know the velocity distribution functions with respect to the magnetic field direction. Such distributions are depicted in Figure 3-4, where $f(v_\perp)$ and $f(v_\parallel)$ are shown with subscripts referring to the direction of the magnetic field. Again the distributions are depicted at different positions within the shock. They are calculated in the same manner as the spherical distribution function and are normalized to the same ordinate value. At z = 84, the front of the shock, almost all particles have velocity $v_\perp = 2000$ km/sec, $v_\parallel = 0$. On considering the distribution function at values of z = 94, 104, and 112 cells, we see that the $v_\perp$ distribution has relaxed and that the $v_\parallel$ distribution has developed a Maxwellian form. From the standpoint of developing a kinetic theory of the plasma instabilities responsible for these observed velocity space distributions, it is important to note that is that *the $v_\perp$ distribution retains a "shell-like" form well into the shock.* Thus, at least for the case of dynamically produced collisionless shocks such as the one simulated here, it is not appropriate to model shock instabilities with a simple bimaxwellian velocity distribution such as is used in the bulk of analyses of thermalizing instabilities in collisionless shocks.

Summary of observations: We have simulated a collisionless shock wave typical of HANE conditions and observed its interaction with particles. We saw that particles are strongly accelerated when they encounter the shock, with some fraction of them reflected back from the shock front. As one proceeds deeper and deeper into the shocked plasma, the particular distribution functions were observed to undergo a two stage relaxation process. Over a relatively short distance, the particles are strongly scattered in the plane perpendicular to the magnetic field and the distribution function becomes gyrotropic. Over a longer distance scale, the velocity components perpendicular and parallel to the magnetic field also relax. The parallel distribution, originally a spike at $v_\parallel = 0$, becomes Maxwellian as perpendicular energy is scattered into parallel energy. The perpendicular distribution, originally a beam with $v_\perp = v_{\perp0}$ relaxes strongly but retains a distinct shell-like character.
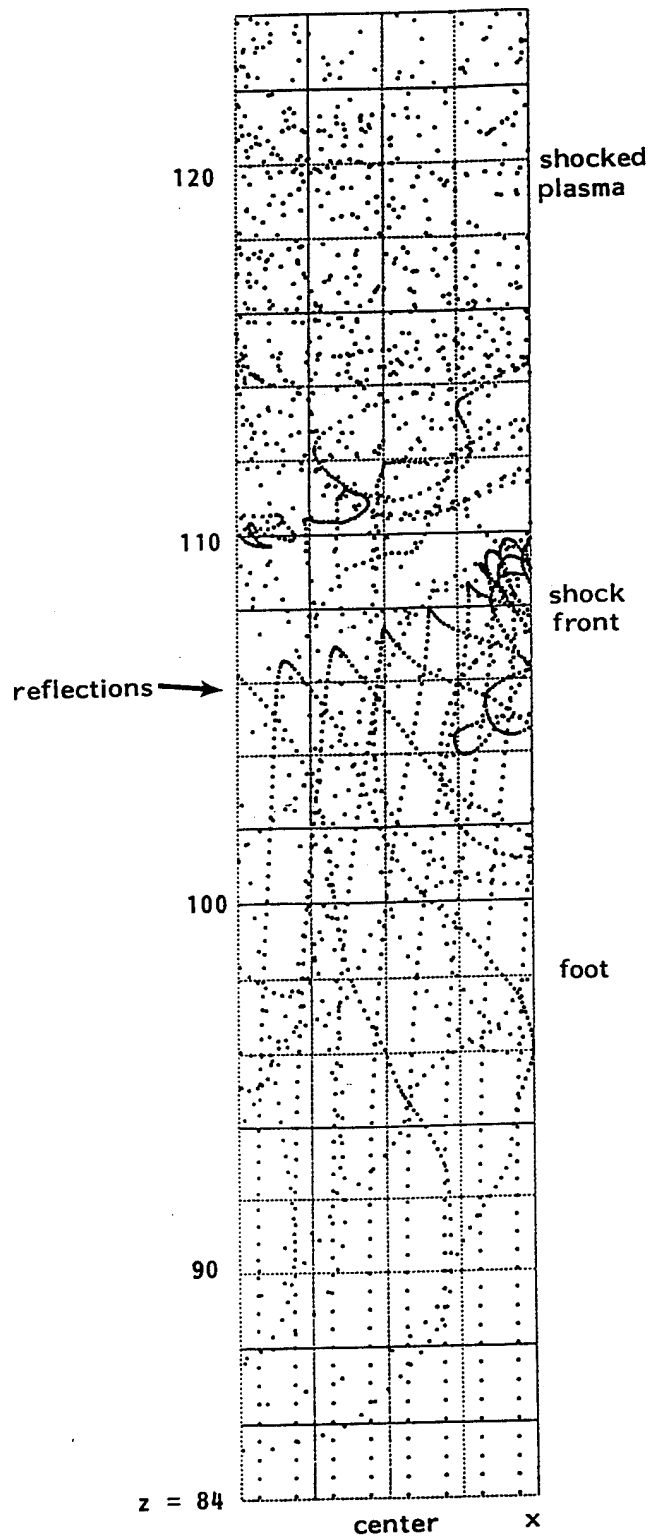
Figure 3-1.   Individual particle positions in 2 cell × 20 cell region.

{cell, number of particles}

{84, 614}

f(v)

1000 2000 3000 4000 5000
v

(a)

0

θ

π

φ

0

2π

{88, 935}

1000 2000 3000 4000 5000

(b)

{92, 1897}

1000 2000 3000 4000 5000

(c)
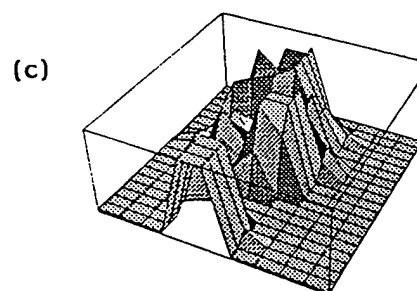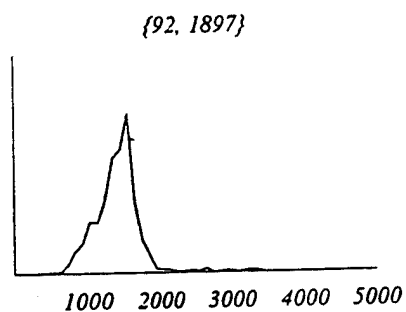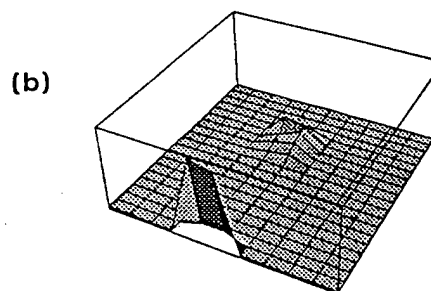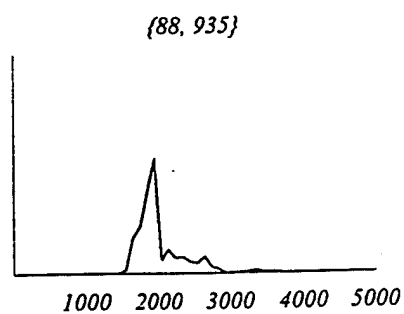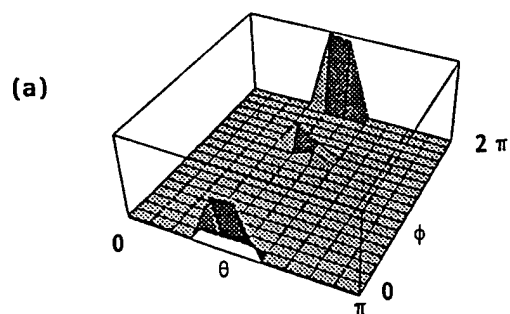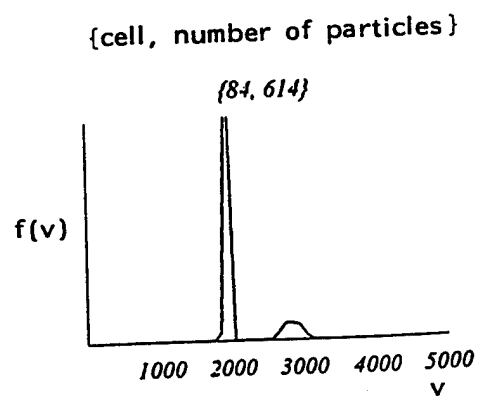
Figure 3-2.   Spherical representation of velocity distribution function at three points successive deeper into the shocked plasma. A rapid evolution of particle velocity distribution from beam to gyrotropic form is observed.

11

(a)

B

X

θ

beam-like

$f(\theta, \phi)$

z φ

(b)
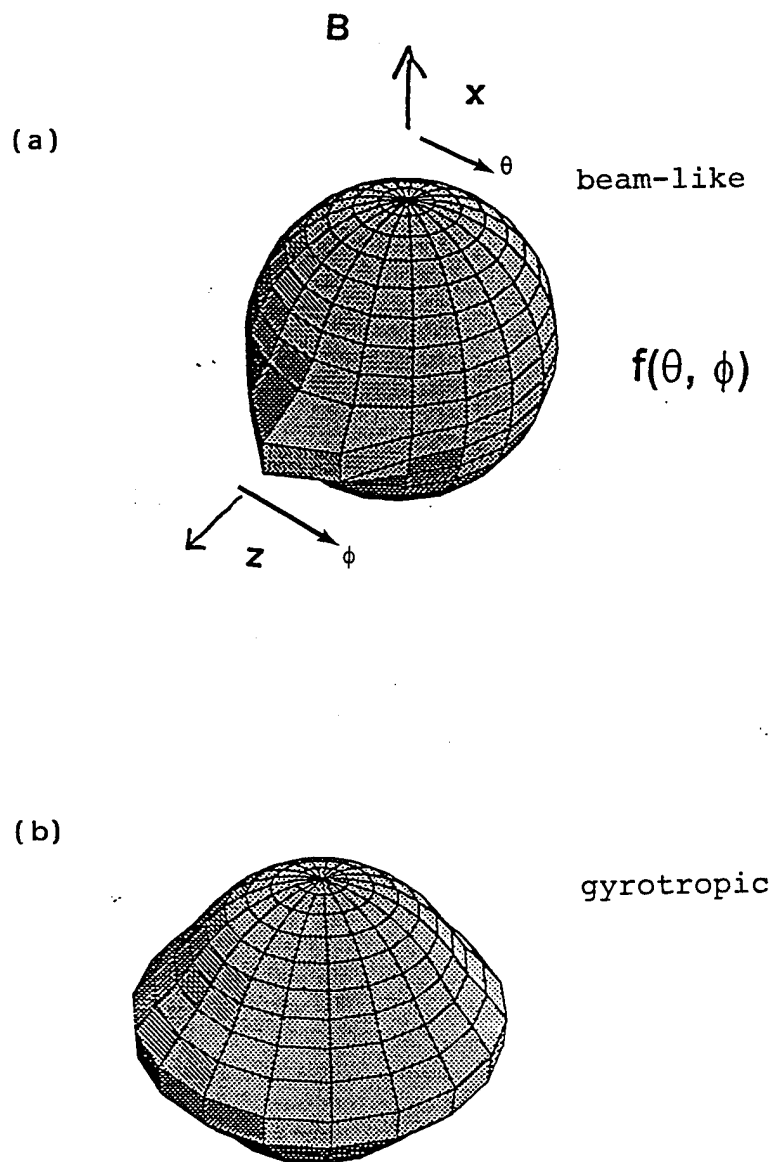
gyrotropic

Figure 3-3.   Spherical perspective plots showing what is meant by evolution from beam-like to gyrotropic distribution.

{z-cell, number of particles}
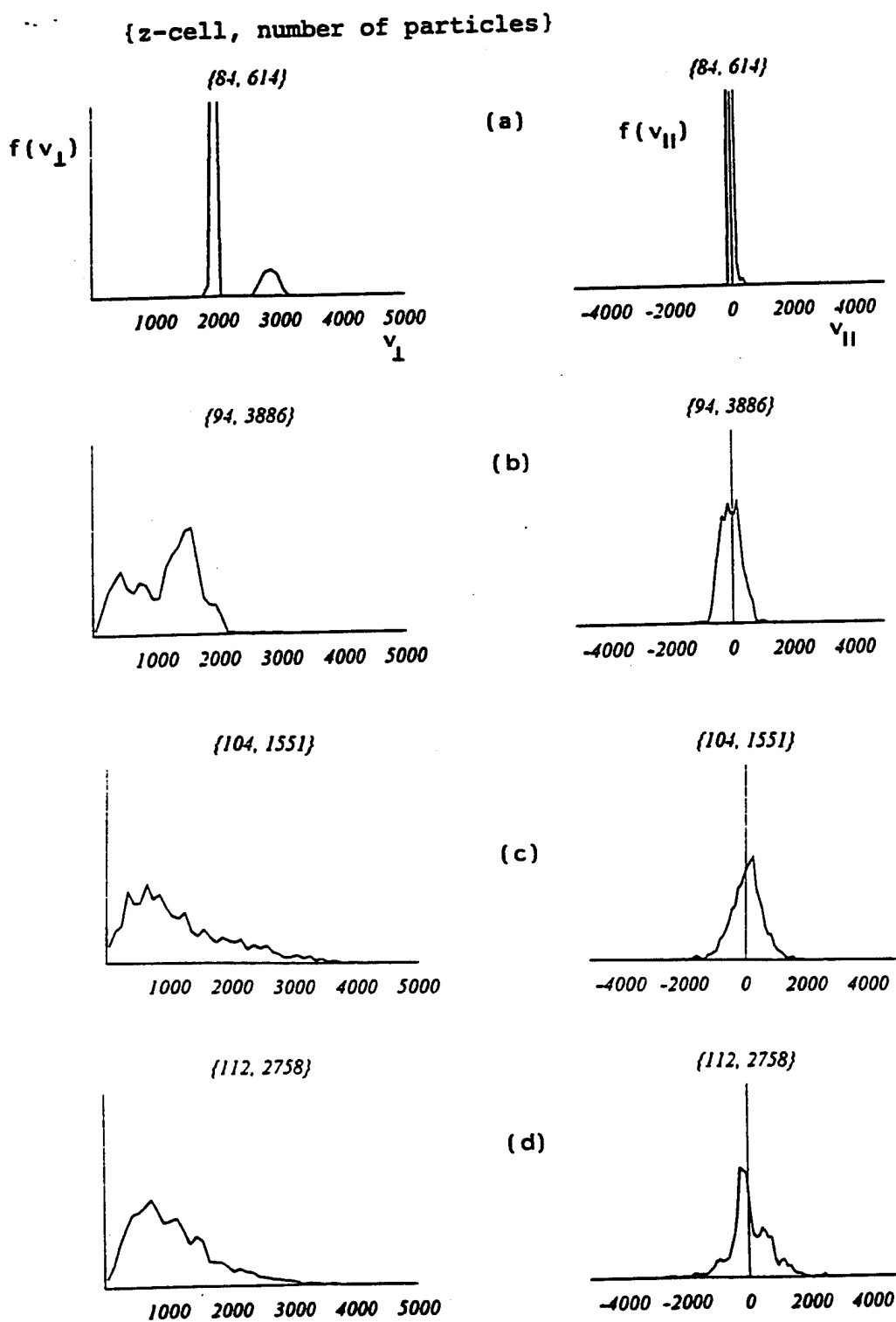
Figure 3-4. Longer time scale evolution of beam-like velocity distribution to form which is Maxwellian in $v_{\parallel}$ and shell-like in $v_{\perp}$. Shown is a sequence of distributions that are successively deeper into the shocked plasma.

13

SECTION 4
VELOCITY DISTRIBUTION FUNCTION FOR
PARTICLES ENCOUNTERING COLLISIONLESS SHOCK

To model the shell-like $v_\perp$ distribution observed in the simulation of a collisionless shock we choose the functional form

$$f(v_\perp, v_\parallel) \sim Exp[-V_\parallel^2] \, Exp[-(V_\perp - V_0)^2] \tag{4.1}$$

where $V_\perp = v_\perp/v_{t\perp}$, $V_\parallel = v_\parallel/v_{t\parallel}$, $V_0 = v_0/v_{t\perp}$. Here the parameter v_0 characterizes the shell-like form of the distribution, while $v_{t\perp}$ and $v_{t\parallel}$ model the thermal spread in the directions perpendicular and parallel to the magnetic field. When this distribution is normalized, $2\pi \int v_\perp dv_\perp dv_\parallel f(v_\perp, v_\parallel) = 1$, the perpendicular part can be separated out to illustrate the normalization associated with the shell-like distribution

$$f(v_\perp) = \frac{2 Exp[-(V_\perp - V_0)^2]}{v_{t\perp}^2 [Exp[-V_0^2] + \sqrt{\pi} V_0 (1 + Erf(V_0))]} \tag{4.2}$$

This is characterized by the two parameters v_0 and $v_{t\perp}$. To demonstrate that this is a reasonable choice for representing the shell-like $v_\perp$ equilibrium we show, in Figure 4.1, the result of fitting the distribution (2) to the observed $f(v_\perp)$ distribution at $z = 96$ and 104 cells. The fitting was achieved with a nonlinear least-squares method using v_0 and $v_{t\perp}$ as parameters. Specifically, both distributions were normalized and then a function $Err(v_0, v_{t\perp}) = \sum [(f(v_0, v_{t\perp}, v_\perp) - f_{obs}(v_\perp)]^2$ was constructed to measure the error between the analytical distribution and the observed distribution. The sum is over available $v_\perp$ data points. $Err(v_0, v_{t\perp})$ was then numerically minimized with respect to its parameters with the minimizing values of v_0 and $v_{t\perp}$ providing the best fits to the data. Notice that the distribution in Figure 4.1b), which is measured some 8 cells further into the shocked plasma than the distribution in Figure 4.1a), has relaxed its shell-like character (v_0 is less) and is more thermal ($v_\perp$ is greater).

Moments: For purposes of reference we calculate some moments of this distribution. The perpendicular speed moment is given by

$$\langle V_\perp f \rangle = \frac{2V_0 + \sqrt{\pi} \, Exp(V_0^2)(1 + 2V_0^2)(1 + Erf(V_0))}{2[1 + \sqrt{\pi} \, Exp(V_0^2) V_0 (1 + Erf(V_0))]} \tag{4.3}$$

where $\langle x \, f \rangle \equiv 2\pi \int v_\perp dv_\perp dv_\parallel \, x \, f(v_\perp, v_\parallel)$. The perpendicular temperature moment is given by

$$\langle V_\perp^2 f \rangle = \frac{2(1 + V_0^2) + \sqrt{\pi}\ Exp(V_0^2)V_0(3 + 2V_0^2)(1 +}{2[1 + \sqrt{\pi}\ Exp(V_0^2)V_0(1 + Erf(V_0))]} \tag{4.4}$$

These moments collapse back to the expected Maxwellian forms when $V_0 \to 0$.

(a)

z-cell = 96

v_0 = 1008 km/sec

$v_{t\perp}$ = 900 km/sec

(b)

z-cell = 104

v_0 = 988 km/sec
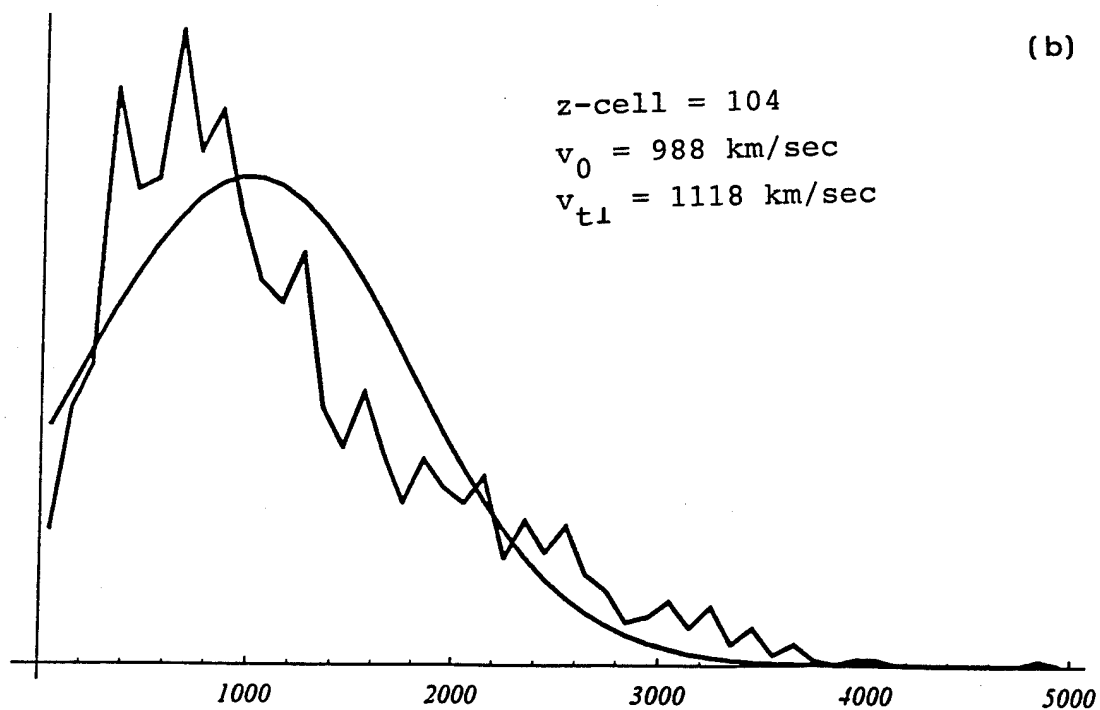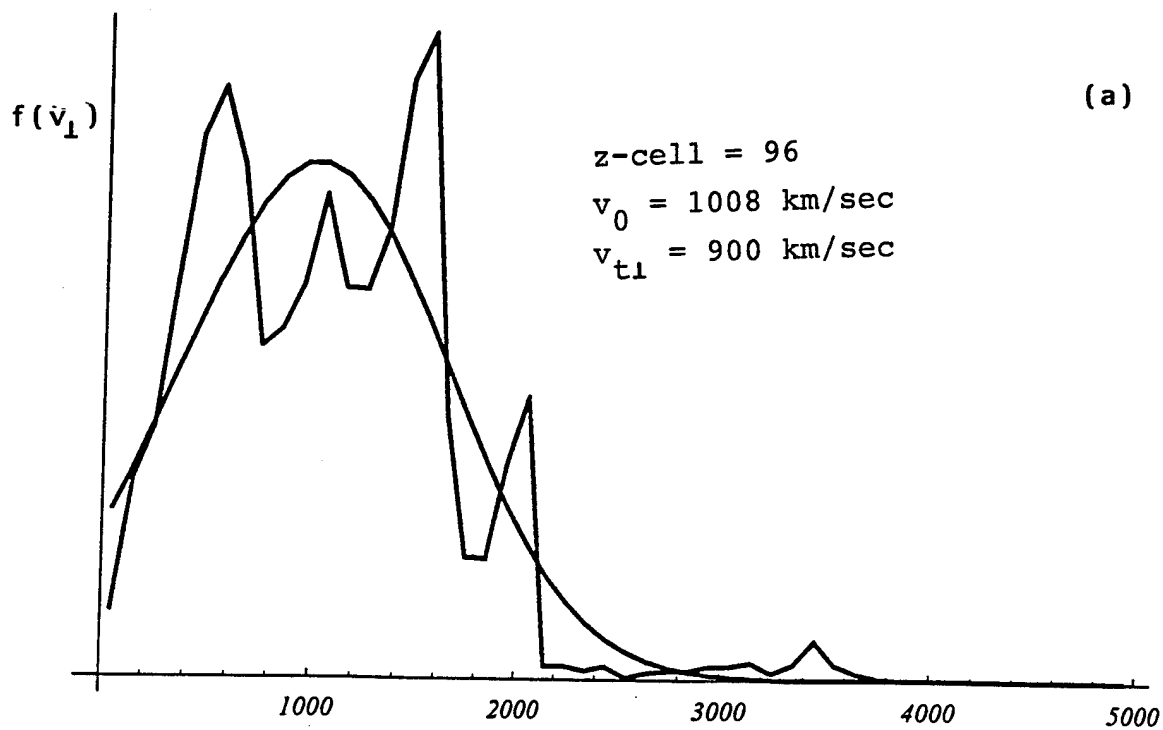
$v_{t\perp}$ = 1118 km/sec

Figure 4-1.   Example of nonlinear least-squares fits of analytic $v_\perp$ velocity distributions with observed distributions at two positions successively deeper into the shock.

16

SECTION 5
SUMMARY AND CONCLUSIONS

A two-dimensional hybrid particle-in-cell simulation has been used to study the velocity distribution functions of a plasma shocked by collisionless shock wave typical of a HANE expansion. Such distribution functions are fundamentally important in ascertaining the dispersive and growth properties of plasma instabilities that regulate the flow of energy away from a HANE. Previously, these instabilities have been primarily studied for the bi-Maxwellian velocity distributions that are thought to be typical of the steady state collisionless bow shock formed where the solar wind encounters the Earth's magnetic field. The collisionless shock formed by a HANE, on the other hand, is dynamic and would be expected to lead to velocity distributions more severely distorted than the bimaxwellians on which most stability analysis is based.

In the simulation, it was observed that background particles are strongly accelerated on encountering the shock front. Because of the irregular nature of the shock front, the acceleration does not take the form of a specular reflection often associated with collisionless shocks based on 1-D analysis and simulation (Winske and Quest, 1988). Rather the acceleration occurs in various directions with respect to the shock front. Some of the belief that particles should specularly reflect from a collisionless shock stems from their study with 1-D simulations in which the spatial structure in directions perpendicular to shock propagation are not considered. By examining the velocity distribution with respect to the distance within the shock, we can study the evolution of the initially beam-like velocity distribution (with respect to the shock front). It was found that the most rapid evolution of the distribution was a rapid relaxation to a gyrotropic form, i.e., a form that was independent with respect to angle about the magnetic field. Over a somewhat longer distance scale, the distribution began to develop a Maxwellian form with respect to velocities parallel to the magnetic field.

The most significant finding of this study was that the velocity distribution perpendicular to the magnetic field did not have a Maxwellian form but maintains a distinct shell-like form with respect to $v_\perp$. We found that the observed distribution could be fitted reasonably well (nonlinear χ^2) with the functional form $f_0(v_\perp) \sim \exp[-(v_\perp - v_0)^2]$.

In a companion report [Gladd and Brecht, 1994], we examine the implications of such a shell-like distribution function for the mirror mode and Alfven ion cyclotron instabilities that are considered to be the most important mechanisms for isotropizing plasma energy. For bimaxwellian velocity distributions, the Alfven ion cyclotron is known to be more important than the mirror mode. The principle finding in Gladd and Brecht, 1994, is that, despite the shell-like velocity distribution, the Alfven ion cyclotron instability still dominates the mirror mode instability in thermalizing the anisotropic plasma produced by a collisonless shock.

SECTION 6
REFERENCES

Ambrosiano, J., and S. H. Brecht, *A simulation study of the Alfven ion cyclotron instability in high beta plasmas*(U), Phys. Fluids, **30**, 108, 1987. (UNCLASSIFIED)

Anderson, B. G. and S. A. Fuselier, *Magnetic pulsations form 0.1 to 4.0 Hz and associated plasma properties in the Earth's sub-solar magnetosheath and plasma depletion layer*(U), J. Geophys. Res. **98**, 1461, 1993. (UNCLASSIFIED)

Barnes, A., *Collisionless damping of hydromagnetic waves*(U), Phys.Fluids **9**, 1483, 1966. (UNCLASSIFIED)

Brecht, S. H. and V. A. Thomas, *Multidimensional simulations using hybrid particle codes*(U), Computer Physics Communications **48**, 135, 1988. (UNCLASSIFIED)

Brinca, A. L., N. Sckopke and G. Paschmann, *Wave excitation downstream of the low-β, quasi-perpendicular bow shock*(U), J. Geophys. Res., **95**, 6331, 1990. (UNCLASSIFIED)

Brinca, A. L., L. Borda de Agua, and D Winske, *Nongyrotropy as a source of instability and mode coupling*(U), Geophys. Res. Lett., **12**, 2445, 1992. (UNCLASSIFIED)

Chandrasekhar, S., A. N. Kaufman, and K. M Watson, *The stability of the pinch*(U), Proc. Royal Soc. London, Ser. A, **245**, 435, 1958. (UNCLASSIFIED)

Davidson, R. C. and Ogden, J. M., *Electromagnetic ion cyclotron instability driven by ion energy anisotropy in high-beta plasmas*(U), Phys. Fluids **18**, 1045, 1975. (UNCLASSIFIED)

Gary, S. P., M. D. Montgomery, W. C. Feldman, and D. W. Forslund, *Proton temperature anisotropy instabilities in the solar wind*(U), J. Geophys. Res., **81**, 1241, 1976. (UNCLASSIFIED)

Gary, S. P., *The mirror and ion cyclotron instabilities*(U), J. Geophys. Res., **97**, 8519, 1992. (UNCLASSIFIED)

Gladd, N.T. and Stephen H. Brecht, *Thermalizing instabilities in a HANE disturbed plasma*(U), DNA-TR-160, 1994. (UNCLASSIFIED)

Hasegawa, A., *Plasma instabilities and nonlinear effects*(U), Springer-Verlag, New York, 1975. (UNCLASSIFIED)

Kennel, C. F. and H. E. Petschek, (U), J. Geophys. Res. **71**, 1, 1966. (UNCLASSIFIED)

Hubert, D. C. Perche, C. C. Harvey, C. Lacombe, and C. T. Russell, *Observation of mirror waves downstream of a quasi-perpendicular shock*(U), Geophys. Res. Lett. **16**, 159, 1989. (UNCLASSIFIED)

McKean, M. E., D. Winske and S. P. Gary, *Mirror and ion cyclotron anisotropy instabilities in the magnetosheath*(U), J. Geophys. Res., **97**, 19421, 1992. (UNCLASSIFIED)

Moustaizis, S., D. Hubert, A. Mangeney, C. C. Harvey, C. Perche, and C. T. Russell, *Magnetohydrodynamic turbulence in the Earth magnetosheath*(U), Ann. Geophys. **4A**, 355, 1986. (UNCLASSIFIED)

Sckopke, N., G. Paschmann, A. L. Brinca, C. W. Carlson, and H. Luhr, *Ion thermalization in quasi-perpendicular shocks involving reflected ions*(U), J. Geophys. Res, **95**, 6337, 1990. (UNCLASSIFIED)

Tajima, T., K. Mima, and J. M. Dawson, *Alfven ion-cyclotron instability: Its physical mechanism and observation in computer simulation*(U), Phys. Rev. Lett. **39**, 201, 1977. (UNCLASSIFIED)

Thomas, V. A. and S. H. Brecht, *Two dimensional simulation of high Mach number plasma interaction*(U), Phys. Fluids **29**, 2444, 1986. (UNCLASSIFIED)

Tsurutani, B. T., E. J. Smith, R. R. Anderson, K. W. Ogilvie, J. D. Scudder, D. N. Baker, and S. J. Bame, *Lion roars and nonoscillatory drift mirror waves in the magnetosheath*(U), J. Geophys. Res., **87**, 6060, 1982. (UNCLASSIFIED)

Winske, D., and K. B. Quest, *Magnetic field and density fluctuations at perpendicular supercritical collisionless shocks*(U), J. Geophys. Res., **93**, 9681, 1988. (UNCLASSIFIED)

Yoon, P. H., *Quasi-linear evolution of Alfven-ion-cyclotron and mirror instabilities driven by the ion temperature anisotropy*(U), Phys. Fluids **B4**, 3627, 1992. (UNCLASSIFIED)

DISTRIBUTION LIST

DNA-TR-94-161

DEPARTMENT OF DEFENSE

BALLISTIC MISSILE DEFENSE ORGANIZATION
    ATTN: EN LTC C JOHNSON
    ATTN: TN/S

DEFENSE INFORMATION SYSTEMS
    ATTN: SSS

DEFENSE INTELLIGENCE AGENCY
    ATTN: DC-6
    ATTN: DIR
    ATTN: DIW-4
    ATTN: DT-1B

DEFENSE NUCLEAR AGENCY
    ATTN: NASC MARTIN
    ATTN: NASF
    ATTN: OPNA
    ATTN: RAEM
10 CY ATTN: RAEM B PRASAD
    ATTN: RAEM K SCHWARTZ
    ATTN: RAES
    ATTN: RAST K WARE
    ATTN: RAST W SUMMA
    ATTN: SPSD
    ATTN: SPWE R COX
2 CY ATTN: SSTL

DEFENSE TECHNICAL INFORMATION CENTER
2 CY ATTN: DTIC/OC

FIELD COMMAND DEFENSE NUCLEAR AGENCY
    ATTN: FCPRA
    ATTN: FCTO

JOINT STAF/J-3
    ATTN: J36 CCD

TECHNICAL RESOURCES CENTER
    ATTN: JNGO

U S NUCLEAR COMMAND & CONTROL SYS
SUPPORT STAFF
    ATTN: DR S HO
    ATTN: SAB H SEQUINE

DEPARTMENT OF THE ARMY

ADVANCED RESEARCH PROJECT AGENCY
    ATTN: CHIEF SCIENTIST

ARMY LOGISTICS MANAGEMENT CTR
    ATTN: DLSIE

U S ARMY COMM R&D COMMAND DEFENSE CMD
    ATTN: CSSD-SA-E
    ATTN: CSSD-SA-EV

U S ARMY COMMUNICATIONS R&D COMMAND
    ATTN: AMSEL-RD-ESA

U S ARMY ENGINEER DIV HUNTSVILLE
    ATTN: PRESTON J KISS

U S ARMY NATIONAL GROUND INTELLIGENCE CENTER
    ATTN: IAFSTC-RMT

U S ARMY NUCLEAR & CHEMICAL AGENCY
    ATTN: MONA-NU DR D BASH

U S ARMY TRADOC ANALYSIS CTR
    ATTN: ATAA-PL
    ATTN: ATAA-TDC
    ATTN: ATRC-WCC L DOMINGUEZ

DEPARTMENT OF THE NAVY

NAVAL OCEAN SYSTEMS CENTER
    ATTN: CODE 542 J FERGUSON

NAVAL RESEARCH LABORATORY
    ATTN: CODE 4183
    ATTN: CODE 5326 G A ANDREWS
    ATTN: CODE 5340 E MOKOLE
    ATTN: CODE 6750 P RODRIGUEZ
    ATTN: CODE 6790 DR J HUBA
    ATTN: CODE 6790 DR P BERNHARDT
    ATTN: CODE 7604 H HECKATHORN
    ATTN: JACOB GRUN CODE 6790

DEPARTMENT OF THE AIR FORCE

AFIWC/MSO
    ATTN: SAVC
    ATTN: SAZ

AIR UNIVERSITY LIBRARY
    ATTN: AUL-LSE

DNA-USSTRATCOM/SPACECOM/ACC
    ATTN: DNA LIAISON
    ATTN: J61
    ATTN: USSTRATCOM/J5

NATIONAL TEST FACILITY/ENC
    ATTN: NTF/EN MAJ VAN FOSSON

PHILLIPS LABORATORY/GPOS
    ATTN: OP DR W BLUMBERG

DEPARTMENT OF ENERGY

EG&G, INC
    ATTN: D WRIGHT

SANDIA NATIONAL LABORATORIES
    ATTN: ORG 9110 G CABLE
    ATTN: ORG 9110 W D BROWN
    ATTN: TECH LIB 3141

OTHER GOVERNMENT

CENTRAL INTELLIGENCE AGENCY
    ATTN: OSWR/NED 5S09 NHB
    ATTN: OSWR/SSD L BERG

DEPARTMENT OF DEFENSE CONTRACTORS

AEROSPACE CORP
    ATTN: BRIAN PURCELL
    ATTN: C CREWS
    ATTN: C RICE
    ATTN: DR J M STRAUS
    ATTN: M ROLENZ

AUSTIN RESEARCH ASSOCIATES
    ATTN: R THOMPSON

AUTOMETRIC, INC
    ATTN: C LUCAS

BDM FEDERAL INC
    ATTN: W LARRY JOHNSON

BERKELEY RSCH ASSOCIATES, INC
    ATTN: J WORKMAN
2 CY ATTN: N T GLADD
2 CY ATTN: S BRECHT

DELVIN SYSTEMS
    ATTN: B PHILLIPS
    ATTN: N CIANOS

ELECTROSPACE SYSTEMS, INC
    ATTN: LINDA CALDWELL

GRUMMAN AEROSPACE CORP
    ATTN: J DIGLIO

HORIZONS TECHNOLOGY, INC
    ATTN: B LEE

INSTITUTE FOR DEFENSE ANALYSES
    ATTN: E BAUER
    ATTN: H WOLFHARD

JAYCOR
    ATTN: CYRUS P KNOWLES

KAMAN SCIENCES CORP
    ATTN: DASIAC

KAMAN SCIENCES CORPORATION
    ATTN: B GAMBILL
    ATTN: DASIAC
    ATTN: R RUTHERFORD

LOCKHEED MISSILES & SPACE CO, INC
    ATTN: J KUME

LOGICON R & D ASSOCIATES
    ATTN: S WOODFORD

LOGICON R & D ASSOCIATES
    ATTN: E HOYT

MISSION RESEARCH CORP
    ATTN: R ARMSTRONG
    ATTN: W WHITE

MISSION RESEARCH CORP
    ATTN: R L BOGUSCH

MISSION RESEARCH CORP
    ATTN: DAVE GUICE

MISSION RESEARCH CORP
    ATTN: B R MILNER
    ATTN: D KNEPP
    ATTN: D LANDMAN
    ATTN: F GUIGLIANO
    ATTN: R BIGONI
    ATTN: R DANA
    ATTN: R HENDRICK
    ATTN: S GUTSCHE
    ATTN: TECH LIBRARY

MISSION RESEARCH CORP
    ATTN: B WORTMAN

MITRE CORPORATION
    ATTN: G COMPARETTO

NORTHWEST RESEARCH ASSOC, INC
    ATTN: E FREMOUW

PACIFIC-SIERRA RESEARCH CORP
    ATTN: R BUCKNER

PACIFIC-SIERRA RESEARCH CORP
    ATTN: E FIELD
    ATTN: H BRODE
    ATTN: R LUTOMIRSKI

PACIFIC-SIERRA RESEARCH CORP
    ATTN: M ALLERDING

PHOTOMETRICS, INC
    ATTN: I L KOFSKY

ROCKWELL INTERNATIONAL CORPORATION
    ATTN: J AASTERUD
    ATTN: TECH LIBRARY

SCIENCE APPLICATIONS INTL CORP
    ATTN: D SACHS
2 CY ATTN: L LINSON

SPARTA INC
    ATTN: D DEAN

SRI INTERNATIONAL
    ATTN: W CHESNUT

TELEDYNE BROWN ENGINEERING
    ATTN: J FORD
    ATTN: J WOLFSBERGER JR

TOYON RESEARCH CORP
    ATTN: J ISE

TRW INC
    ATTN: TIC

TRW SPACE & DEFENSE SECTOR
    ATTN: D M LAYTON

VISIDYNE, INC
    ATTN: J CARPENTER
    ATTN: J DEVORE
    ATTN: J THOMPSON
    ATTN: W SCHLUETER